



Infrared visualization of thermal motion inside a sessile drop deposited onto a heated surface

D. Brutin*, B. Sobac, F. Rigollet, C. Le Niliot

Aix-Marseille Université (U1-U2), Laboratoire IUSTI, Technopôle de Château-Gombert, 5 rue Enrico Fermi, 13453 Marseille, France

ARTICLE INFO

Article history:

Received 7 October 2010
Received in revised form 13 December 2010
Accepted 13 December 2010
Available online 19 December 2010

Keywords:

Sessile drops
Convection cells
Evaporation
Infrared camera
Thermal motion
Spectroscopy

ABSTRACT

Drop evaporation is a basic phenomenon but the mechanisms of evaporation are still not entirely clear. A common agreement of the scientific community based on experimental and numerical work is that most of the evaporation occurs at the triple line. However, the rate of evaporation is still predicted empirically due to the lack of knowledge of the governing parameters on the heat transfer mechanisms which develop inside the drop under evaporation. The evaporation of a sessile drop on a heated substrate is a complicated problem due to the coupling by conduction with the heating substrate, the convection/conduction inside the drop and the convection/diffusion in the vapor phase. The coupling of heat transfer in the three phases induces complicated cases to solve even for numerical simulations. We present recent experimental results obtained using an infrared camera coupled with a microscopic lens giving a spatial resolution of 10 μm to observe the evaporation of sessile drops in infrared wavelengths. Three different fluids fully characterized, in the infrared wavelengths of the camera, were investigated: ethanol, methanol and FC-72. These liquids were chosen for their property of semi-transparency in infrared, notably in the range of the camera from 3 to 5 μm . Thus, it is possible to observe the thermal motion inside the drop. This visualization method allows us to underline the general existence of three steps during the evaporating process: first a warm-up phase, second (principal period) evaporation with thermal-convective instabilities, and finally evaporation without thermal patterns. The kind of instabilities observed can be different depending on the fluid. Finally, we focus on the evolution of these instabilities and the link with the temperature difference between the heating substrate and the room temperature.

© 2010 Elsevier Inc. All rights reserved.

1. State of the art

Drop evaporation has been widely investigated theoretically [1], experimentally [2,3] and numerically [4]. Generally, the work deals with either drops with small sizes [5,6] or flat drops which can be comparable with films [7]. Table 1 summarizes numerous studies of drop and droplet evaporation performed since 1973; most of these studies discuss physical mechanisms related to the evaporation dynamics. Scientific production has sharply increased since 1995. Indeed, drop and droplet evaporation is involved in many industrial processes and in many heat and mass transfer applications. The literature evidences that the main physical mechanisms driving droplet evaporation are the following:

- the heat transfer by conduction in the substrate,
- the heat transfer by convection [temperature gradients induces superficial tension gradients (Marangoni effects) and normal convection],

- the liquid/substrate molecular interaction at the roughness scale that tends to modify the wettability of the drop for a given drop volume,
- the vapor mass diffusion around the drop.

In spite of the considerable activity attested by the large quantity of publications, the dominant mechanisms acting on the kinetics of drop evaporation are not well understood because of the strong coupling between the various phenomena. In the studies of drop evaporation, two approaches can be distinguished: drop evaporation either with [13,18] or without [15] wall heating. Without wall heating, the drop evaporation dynamic is slower compared to the heating situation. Also, the wall heating enables a higher evaporation flow rate inducing a high temperature gradient inside the drop; this last situation is useful when working with a given infrared resolution.

In an unsaturated atmosphere and without overheating from the substrate, the mass diffusion of the vapor in the gas surrounding the droplet can become the limiting phenomenon of evaporation kinetics. According to the experiments of Shahidzadeh-Bonn et al. [30], such a phenomenon is much more pronounced for organic fluids than for water, this being mainly due to the difference of densities

* Corresponding author. Tel.: +33 491106886; fax: +33 491106969.
E-mail address: david.brutin@polytech.univ-mrs.fr (D. Brutin).

Nomenclature

Roman letters

C_p	heat capacity ($\text{J kg}^{-1} \text{K}^{-1}$)
d	drop base diameter (mm)
g	gravitational constant (9.81 m s^{-2})
h	drop height (mm)
k	absorption coefficient (m^{-1})
L_c	capillary length (mm)
L_v	latent heat of vaporization (kJ kg^{-1})
L	luminance ($\text{W m}^{-2} \text{s r}^{-1} \mu\text{m}^{-1}$)
m	drop mass (μg)
P	heat power (W)
Q	heat flux (W m^{-2})
R	drop base radius (mm)
S	surface (m^2)
t	time (s)
T	temperature ($^{\circ}\text{C}$)
V	drop volume (μL)

Dimensionless numbers

Bo	Static Bond number (–)
Ma	Marangoni number (–)
Nu	Nusselt number (–)
Pr	Prandtl number (–)
Ra	Rayleigh number (–)

Greek symbols

α	thermal diffusivity ($\text{m}^2 \text{s}^{-1}$)
β	coefficient of thermal expansion (K^{-1})
Δ	difference (–)
ϵ	emissivity (–)
λ	heat conductivity ($\text{W m}^{-1} \text{K}^{-1}$)
μ	dynamic viscosity (Pa s)
ν	kinematic viscosity ($\text{m}^2 \text{s}^{-1}$)
ρ	density (kg m^{-3})
σ	surface tension (N m^{-1})
τ	transmittivity (–)
θ	contact angle ($^{\circ}$)

Subscripts and superscripts

Conv	convection
Drop	drop
L	liquid
S	sensor
Sat	saturation
Sub	substrate
SW	short wave (range of 3–5 μm)
V	vapor

between vapor and air. In the cases of drops on a heated substrate, the interactions between the liquid and the substrate play a fundamental role in the evaporation kinetics. A significant difference in temperature between the substrate and the liquid is a source of thermo-convective instabilities induced by the Marangoni effect and buoyancy forces. These instabilities depend mainly on the thermophysical properties of the liquid and the substrate, but also on the drop shape which is correlated with interactions at the liquid/substrate interface.

The experimental studies summarized in Table 1 attempt to explain the role of the mechanisms specific to drop evaporation. The parameters of the drop (radius, height and contact angle) are

usually deduced by visualization using a visible camera. Thus the behavior of drops for various liquid/substrate combinations have been analyzed by several authors under various experimental conditions. Two modes of evaporation are observed: one with a pinned diameter and one with constant angle of contact and both appearing in sequences. Crafton and Black [16] observed that for a water drop the basic radius of the drop remains constant during evaporation, whereas for a heptane drop the contact angle remains constant. Other observations on the rate of evaporation of the drops (based on the measurement of volume or weight variation) indicate a linear relation between the rate of evaporation and the wetting diameter of the drops [7,16,18].

Table 1
Articles related to drop evaporation (several approaches are presented: experiments, numerical simulations, theoretical approaches) (Exp.: experimental work; Num.: numerical simulations; Th.: theoretical work; SS: stainless steel).

Authors [Ref.]	Year	Approach	Fluid	Substrate
Boyes [8]	1973	Exp.	Water with saturated vapor	Cu, PTFE
Piknett [9]	1977	Exp.	Methyl-acetoacetate	PTFE
Birdi [2]	1989	Exp.	Water	PTFE
Bourges-Monnier [10]	1995	Num. and exp.	Water, N-decane	PTFE, SiO ₂ , epoxy
Hegseth [11]	1996	Exp.	Ethanol, polystyrene particles	–
Chandra [12]	1996	Exp. and Th.	Water with surfactant	SS
Bernardin [13]	1997	Exp.	Water	Al
Zhang [14]	2002	Exp.	Silicon oil, R113, ethanol	Anodized glass
Hu [5]	2002	Num. and Exp.	Water	Glass
Erbil [15]	2002	Exp.	Butanol, toluene, nonane, octane	PTFE
Crafton [16]	2004	Exp.	Water, N-heptane	Cu, Al
Savino [17]	2004	Exp. and Num.	Silicon oil, hydrocarbons, water	Several metals
Grandas [18]	2004	Exp.	Water	PTFE, Al
Poulard [19]	2005	Exp. and Num.	Water, alkanes	SiO ₂
Frassy [20]	2006	Exp. and Num.	Water	SiO ₂ , silane, polycarbonate
Sodtke [21]	2007	Exp. and Th.	Water with saturated vapor	SS
Tarozzi [22]	2007	Exp.	Water	Black paint on IR materials
Widjaja [23]	2008	Num. and Exp.	Water	–
Sefiane [24]	2008	Exp.	Ethanol, methanol, FC-72	PTFE, ceramic, Ti, Cu
Tartarini [25]	2009	Exp. and Num.	Water	BaF ₂
Barash [26]	2009	Num. and Th.	Toluene	–
Tam [27]	2009	Exp. and Th.	Water	Superhydrophobic surfaces
Dhavaleswarapu [28]	2009	Exp. and Th.	Water	Glass
Nikolayev [29]	2010	Th. and num.	Water	SS

Although the observations using visible camera are useful to give an overall picture of the mass transfer of the drops, such an experimental approach is not sufficient to determine the role of the selected pair liquid/substrate in modeling the internal dynamics of the drop. Few experimental studies attempt to give greater comprehension of the phenomenon of drop evaporation using original techniques. Hegseth et al. [11] and Kang et al. [31] used optical techniques of the PIV type (Particle Imaging Velocimetry) to visualize the fluid motion inside the drop using polystyrene particles in an ethanol drop, whereas Zhang and Chao [14] employed a shadowgraphy laser method. Studies dealing with the phenomena of thermogravitational and thermocapillary convection in a drop deposited onto a silicon surface were carried out by using infrared thermography by Savino and Fico [17]. The distribution of the wall temperature below the drop is also given either by using liquid crystals [21] or by infrared thermography through a transparent substrate [22]. Infrared thermography is generally used to take non-intrusive measurements [22,17,32,33]. The advantage of these techniques is the absence of contact which thus makes it possible to observe the thermal phenomenon without contact. However, the difficulty is then to correctly interpret the infrared information measured by the camera according to the radiative properties of the fluid observed. Indeed, the liquid sample can be semi-transparent in the spectral range of measurement, making it difficult to convert the measured brightness into surface temperature. Some authors [25,22] choose not to observe the fluid directly but prefer to observe the back face on which the drop evaporates. The substrate in BaF_2 is coated with an opaque emissive painting which makes it possible to measure its surface temperature; it is also the temperature of the drop contact area with the substrate. In other publications, the authors observe the fluid [32,33,17]. The authors then assume the opacity of the various fluids observed (water, ethanol, N-pentane) in the long-wave spectral field of the camera (9–10 μm); they need only the emissivity of the liquid to deduce the surface temperature.

Two processes play a role in the evaporation of a drop: the diffusion of molecules into the air from the drop surface and the internal flow inside the drop to bring the fresh liquid to the liquid–vapour interface [34]. In between these two physical phenomena, the solid–liquid contact angle plays an important role in the evaporation rate [12]. The reduction of the contact angle increases the surface of contact between the droplet and surface, and also reduces the drop thickness, thus increasing the contribution of thermal conduction from the substrate to the liquid–gas interface. These two effects increase the rate of evaporation.

A recent study has been performed by Sefiane et al. [24] on the use of thermography to observe a droplet under evaporation. However, the paper does not take into account the fluid radiative properties. Also the use of water for infrared properties is very sensitive since water reflectivity is high and transparency in the infrared wavelength of the FLIR SC3000 is almost zero for fluid thicknesses above 0.2 mm (see Table 3). Furthermore, the temperature scales presented in the figures are not related to the drop shape factor or to the fluid spectral emissivity in the infrared wavelength range of camera. The conclusion on the absence of flow motion inside the water droplet cannot be evidenced since water for this drop thickness (more than 1 mm) is totally opaque. The heat flux received by the infrared camera is a surface radiative heat flux which provides only information from a thin layer below the interface of less than 0.2 mm. Furthermore, all experiments are performed in ambient temperature whereas an investigation of the influence of the substrate temperature on the instabilities is carried out in this study. Finally, we characterize the drop evaporation dynamics using a complementary tool which is the heat fluxmeter to carefully analyse the heat transfer to the drop.

An axisymmetric numerical model has been developed by Ruiz and Black [6] to simulate the evaporation of deposited water drops which takes into account evaporation at the surface and convection of the liquid inside the drop due to Marangoni forces. The circulation of the liquid implies a greater rate of evaporation than the previous models and is in accordance with a linear change of volume according to time. Simulations which include convection in the liquid indicate that the flow has a substantial effect on the distribution of the temperature in the drop. Assuming the existence of internal convection in the drop, the distribution of the temperature is very different from the results predicted by a model based on pure conduction in the drop. Ruiz and Black [6] considered the existence of thermocapillary movements in the drop, which gives a distribution of isotherms completely different from that obtained with only conductive heat transfer inside the droplet. Hu and Larson [5] show with a model that the kinetics of evaporation is almost constant during all the phenomena for drops posed with an initial contact angle of $2\pi/9$. In the three cases [5,6,16], the authors studied the phenomena of evaporation for small drops, where the effect of gravity is negligible compared to the effects of surface tension. The shape of these droplets is comparable to a portion of a sphere. In practice, this assumption is valid only for drops below a critical size.

The whole experimental literature (except [24]) do not actually realize that a complicated and non-axisymmetric flow is possible inside the drop due to thermo-capillary instabilities. The strength of this paper is to visualize and investigate this complicated and non-axisymmetric flow inside the drop under evaporation.

The thermal aspects (heat and mass transfer) of the phenomena have never really been approached in a systematic way and the influence of thermal motion on the evaporation process is very largely unknown. This is why we studied the phenomenon of the evaporation of sessile drops using infrared tools in the case of a broad range of sizes, temperature gradients and liquids.

2. Experimental setup

2.1. Drop evaporation apparatus and methods

An experimental device was set up in order to characterize a drop during its evaporation and to analyze the kinetics as well as the heat transfer associated with this phenomenon. This device includes a substrate where the drop is deposited and an instrumentation dedicated to thermal measurements (temperature, heat flux density). The environmental conditions (temperature, pressure, humidity) are measured continuously.

The heater is an aluminum parallelepipedic block ($50 \times 50 \times 20 \text{ mm}^3$) instrumented inside by two heating cartridges 6.35 mm in diameter. A 1-mm-diameter thermocouple of the K type and a platinum probe (Pt 100) are fixed onto the surface. The latter is coupled with a PID regulator in order to maintain the temperature imposed at the surface of the element (between 25 °C and 100 °C) constant. The thermocouple signal is recorded at 1 Hz. A thin foil flexible heat flux sensor (CAPTEC) consists of a thermoelectric panel laminated between flexible heterogeneous very thin plastic layers and is located between the heating aluminum block and the PTFE substrate. The heat flux signal is very sensitive ($0.7 \mu\text{V W}^{-1} \text{ m}^{-2}$). The total thickness of the fluxmeter is 0.6 mm with a diameter of 10 mm. A T-type thermocouple is located inside the heat fluxmeter and will be used in the next sections to follow the substrate temperature. A final PTFE (Polytetrafluoroethylene) sheet with a thickness of 200 μm is stuck on the fluxmeter; this surface will receive the sessile drop. The PTFE sheet

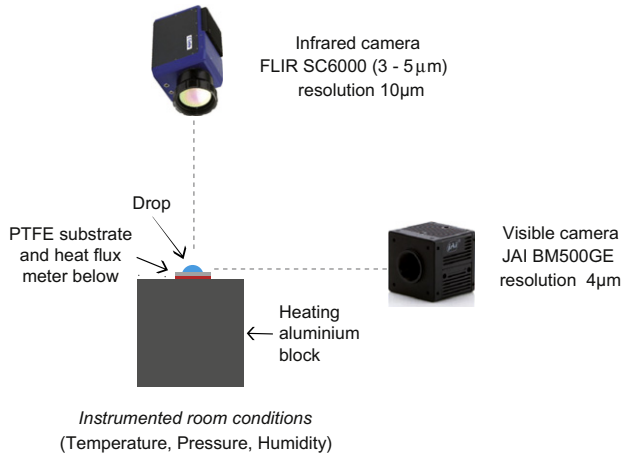


Fig. 1. Experimental setup used for infrared thermography of sessile drop evaporation.

is used for its hydrophobic properties and is changed regularly to avoid the particular problem of cleaning and to guarantee the reproducibility of the surface quality (Fig. 1).

Visible video acquisition is performed using a Pike 800 * 600 pixels camera with 30 images/second coupled to a microscope with a VZM100i lens. This visible imaging allows a visualization of the drop shape from the side. This is used to determine the geometrical parameters of the drop. The sampling rate is 30 images/second because of the low interface displacement velocity. After having selected an area of interest on the image (definition of a base line), an analysis is carried out in order to determine the contact angles on the left and right, the height, the diameter of the wetted area, the external surface and the volume of the drop. The contact angles are given by carrying out a polynomial regression on the drop free interface. Volume is calculated by carrying out an integration with the axisymmetric assumption of drop.

One tool used to analyse flow motion inside a drop measuring a few millimeters in diameter is an infrared camera. Compared to a layer evaporation problem, the first difficulty due to the interface curvature which induces a form factor. This form factor is required to access an accuracy of ± 0.1 °C. For drops, a second difficulty rose, since it is necessary to record the interface with a side view camera over a period of time and then model it in relation to the evaporation of the drop. Then each pixel of the film needs to be computerized with the right total emissivity of the fluid (see Section 2.2.2). This procedure is under implementation. Consequently, the infrared images presented in this work were obtained at half the initial drop thickness. The temperature scale has an uncertainty of ± 0.5 °C. This is a first approach in the analysis of the infrared data. The infrared diagnosis is carried out using a FLIR SC6000 camera (640 * 512 pixels) coupled to a microscope making it possible to reach a resolution of 10 μm , so, a field of view of 6.4 mm * 5.12 mm. The infrared camera is assembled vertically to the top of the drop. Before doing the experiment, it is checked that the substrate temperature homogeneity is stable at ± 0.5 °C.

2.2. Properties of liquids used

2.2.1. Physical properties

Table 2 provides the properties of the fluids investigated in this study and include water properties for comparison. All fluids used have a low surface tension creating drops with a contact angle ranging from 10° to 40° (mainly because of the surface tension: 22.7 mN m⁻¹ for methanol, 12.0 mN m⁻¹ for FC-72 and 22.0 mN m⁻¹ for ethanol). The three fluids have quite different Prandtl numbers [$Pr = (\mu C_p)/\lambda$]. Their heat of vaporization is also very different which makes it possible to observe evaporation over different time ranges and different temperature gradients. The heat of vaporization of FC-72 is very low at 88 kJ kg⁻¹, while for ethanol the heat of vaporization is almost 10 times higher at 841 kJ kg⁻¹; finally the heat of vaporization of methanol is the highest at 1165 kJ kg⁻¹. Ethanol and methanol have almost the same capillary lengths [$L_c = \sqrt{\sigma/(g \cdot \Delta\rho)}$] since their surface tension and fluid and vapor surface tension are similar.

2.2.2. Global emissivity determination

Here is considered a semi-transparent liquid between $x = 0$ and $x = L$. This liquid is homogeneous and is supposed isothermal at temperature T . Furthermore, there is no particle inside that could diffuse radiation. The monochromatic luminance of the entering heat flux (at $x = 0$) and sorting heat flux (at $x = 1$) are respectively noted $L_\lambda(0)$ and $L_\lambda(L)$. The monochromatic transmittivity of the liquid of thickness L is defined by:

$$\tau_\lambda(L, T) = \frac{L_\lambda(L)}{L_\lambda(0)} = e^{-k_\lambda(T) \cdot L} \quad (1)$$

where k_λ (μm^{-1}) is the monochromatic absorption coefficient. The length $1/k_\lambda$ (m) is then the characteristic length of penetration of a wavelength λ radiation. The dimensionless product $k_\lambda \cdot L$ is the monochromatic optical thickness of the liquid. The transmittivity $\tau_\lambda(L)$ is measured by a spectrophotometer and plotted for wavelengths between 3 and 5 μm for three different fluids and for particular thicknesses (Fig. 2).

Due to the hypothesis of non scattering liquid, radiation that is not transmitted through the liquid is only absorbed inside it ($\tau_\lambda(L) + \alpha_\lambda(L) = 1$), the monochromatic absorptivity being noted $\alpha_\lambda(L)$, with $\epsilon_\lambda(L) = \alpha_\lambda(L)$ (Kirchhoff's law). The monochromatic emissivity of the liquid of thickness (L) at temperature (T) is then defined by

$$\epsilon_\lambda(L, T) = 1 - e^{-k_\lambda(T) \cdot L} = 1 - \tau_\lambda(L, T) \quad (2)$$

and is then obtained using the measured value of $\tau_\lambda(L, T)$. If the liquid is transmitting and emitting radiations, the monochromatic luminance of sorting heat flux at $x = L$ is given by

$$L_\lambda(L, T) = L_\lambda(0) e^{-k_\lambda(T) \cdot L} + L_\lambda^0(T) [1 - e^{-k_\lambda(T) \cdot L}] \quad (3)$$

$$L_\lambda(L, T) = \tau_\lambda(L, T) L_\lambda(0) + \epsilon_\lambda(L, T) L_\lambda^0(T) \\ = [1 - \epsilon_\lambda(L, T)] L_\lambda^0(T) + \epsilon_\lambda(L, T) L_\lambda^0(T) \quad (4)$$

After integration on the spectral bandwidth of the infrared camera that is working in the Short Wave range (SW: 3–5 μm), we obtain

Table 2
Physical properties and dimensionless numbers of fluids at 25 °C and 1 atm.

	ρ_L (kg m ⁻³)	ρ_V (kg m ⁻³)	C_p (J kg ⁻¹ K ⁻¹)	L_v (kJ kg ⁻¹)	λ (W m ⁻² K ⁻¹)	μ (mPa s)	σ (mN m ⁻¹)	T_{sat} (°C)	L_c (mm)	Pr (-)
Water	997	0.59	4180	2449	0.606	0.890	72.7	100	2.73	6.14
FC-72	1680	4.35	1100	88.0	0.057	0.638	12.0	56.0	0.82	12.3
Methanol	791	0.21	2531	1165	0.203	0.560	22.7	64.7	1.71	6.98
Ethanol	789	1.50	2845	923	0.140	1.095	22.0	78.0	1.69	22.3

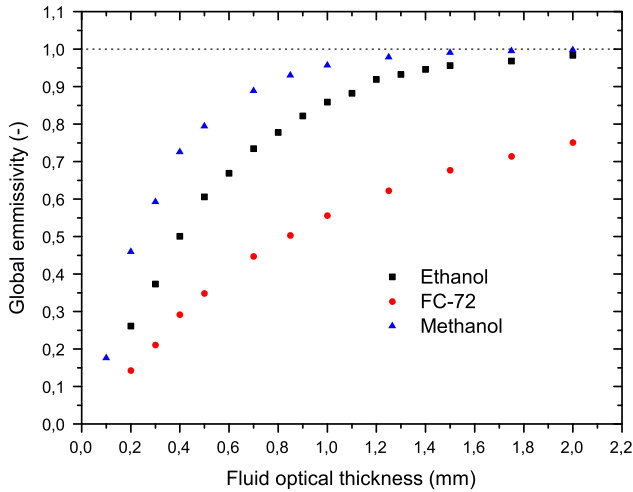


Fig. 2. Global emissivity of FC-72, methanol and ethanol as a function of the optical thickness of the fluid in a wavelength of 3–5 μm ($T_{\text{room}} = 25^\circ\text{C}$, fluid optical thickness uncertainty is $\pm 40 \mu\text{m}$).

$$L_{SW}(L, T) = [1 - \epsilon_{SW}(L, T)]L_{SW}(0) + \epsilon_{SW}(L, T)L_{SW}^0(T) \quad (5)$$

with the ‘global emissivity’ of the liquid layer in the SW range noted $\epsilon_{SW}(L, T)$:

$$\begin{aligned} \epsilon_{SW}(L, T) &= \frac{\int_{\lambda=3}^{\lambda=5} \epsilon_{\lambda}(L, T)L_{\lambda}^0(T)d\lambda}{\int_{\lambda=3}^{\lambda=5} L_{\lambda}^0(T)d\lambda} = \epsilon_{SW}(L, T) \\ &= \frac{\int_{\lambda=3}^{\lambda=5} \epsilon_{\lambda}(L, T)L_{\lambda}^0(T)d\lambda}{L_{SW}^0(T)} \end{aligned} \quad (6)$$

and assuming

$$\frac{\int_{\lambda=3}^{\lambda=5} \epsilon_{\lambda}(L, T)L_{\lambda}(0)d\lambda}{\int_{\lambda=3}^{\lambda=5} L_{\lambda}(0)d\lambda} = \frac{\int_{\lambda=3}^{\lambda=5} \epsilon_{\lambda}(L, T)L_{\lambda}(0)d\lambda}{L_{SW}(T)} \sim \epsilon_{SW}(L, T) \quad (7)$$

Eq. (7) above can describe the situation of a drop (assumed isothermal) deposited onto the heated surface, $L_{SW}(0)$ being the spectral luminance of heat flux leaving the PTFE surface at imposed temperature and $L_{SW}(T)$ being the spectral luminance of heat flux leaving the drop surface toward the infrared camera. The two extreme situations are the following. On one hand, if the liquid layer is completely transparent in the SW bandwidth, $\epsilon_{SW}(L, T) = 0$ and the camera measures directly the heat flux coming from the PTFE heater. On the other hand, if the liquid layer is opaque in the SW bandwidth, $\epsilon_{SW}(L, T) = 1$ and the camera measures only the heat flux coming from the drop surface. The effect of wave reflexions due to change of refractive index at the liquid–gas interface is neglected here. The value of $\epsilon_{SW}(L, T)$ is then the main parameter we need to be able to know at which depth the infrared camera measurement can be associated. In a first approximation in this paper, the temperature scale of infrared images presented here are calculated with this value of global emissivity $\epsilon_{SW}(L, T)$.

The value of $\epsilon_{SW}(L, T)$ measured at 20°C are plotted for three fluids, for several layer thicknesses (Fig. 2). The exponential behaviour expected for the monochromatic value $\epsilon_{\lambda}(L, T)$ according to Eq. (2) is also obtained after integration on the SW bandwidth, it is then

possible to fit the following model on those measurements. The global transmittivity in the SW bandwidth is then obtained as given below:

$$\epsilon_{SW}(L, T) = 1 - e^{-k_{SW}(T)*L} \quad (8)$$

$$\tau_{SW} = 1 - \epsilon_{SW} \quad (9)$$

The obtained values of k_{SW} (mm^{-1}) are presented in Table 3. The dimensionless values of $k_{SW} * L$ indicated for two layer thicknesses (1 and 2 mm) are the optical thicknesses of the liquid layer. The layer is said ‘optically thick’ if its optical thickness is greater than 5 mm, below that value it is semi-transparent. In this table, fluids are listed in order of increasing semi-transparency.

2.2.3. Infrared properties

Three liquids were investigated using the infrared camera: methanol, ethanol and FC-72. All were used for their semi-transparency properties in the infrared wavelength. Measurements were performed using a FTIR NICOLET Nexus 560 spectrophotometer to access the monochromatic transmittivity of a given thickness of fluid in the spectral range of 2.5–14 μm . For the purpose of this study, we analyzed and extracted only the data in the range of 3–5 μm which corresponded to our infrared camera wavelength band. The experimental cell was composed of two CaF_2 windows which were used for their almost total transparency properties in the range of the spectrophotometer. PTFE spacers were used to obtain the adequate optical fluid thickness. Three spacer thicknesses were available: 0.1, 0.2 and 0.5 mm, and could be used together. The optical fluid thickness was deduced on the basis of nine independent measurements of the spacers set using a Mitutoyo CD-15CPX caliper which has an uncertainty of ± 0.02 mm, a resolution of ± 0.01 mm and a repeatability of ± 0.01 mm, and therefore a total uncertainty of ± 0.04 mm. The error bar on the abscissa is the sum of the total uncertainty and the standard deviation of the nine measurements and is about $\pm 40 \mu\text{m}$. The transmittivity measurements were performed three times. For each measurement, a background measurement was first carried out consisting in measuring the radiative power that is transmitted by the cell full of atmospheric air. These three independent measurements provided the ordinate error bar which is the standard deviation.

Ethanol transmittivity in the 3–4 μm range is almost null for a sample fluid with a thickness of 1 mm; then in the range from 4 to 5 μm , the global transmittivity is about 20%. Consequently, the global emissivity for a sample of ethanol with a thickness of 1 mm is 0.859 (Fig. 3). The penetration skin depth of ethanol is 540 μm . For fluid thicknesses below 1.62 mm, emissivity varies exponentially with fluid thickness until a null emissivity for a null fluid thickness. Thus, ethanol can be used for infrared measurement by transmission up to 1.62 mm and have a transmission of 1%.

Fig. 2 provides the global emissivity for the three fluids investigated in the infrared wavelength range: 3–5 μm . The fluid thicknesses investigated range from 0.2 to 2.0 mm, which corresponds to the range of drop height encountered. The drop height being always below the capillary length (L_c). All three emissivity variations in this figure can be fitted by a decreasing exponential law given below:

Table 3
Infrared properties and dimensionless numbers of fluids.

Fluid unit	k_{SW} (mm^{-1})	$1/k_{SW}$ (mm)	$k_{SW}*L$ ($L = 2$ mm) (-)	$k_{SW}*L$ ($L = 1$ mm) (-)	$L_{99\%} = 3/k_{SW}$ (mm)
Water	15.3	0.065	30.7	15.3	0.196
Methanol	3.02	0.33	6.04	3.02	0.994
Ethanol	1.85	0.54	3.70	1.85	1.622
FC-72	0.78	1.28	1.57	0.78	3.847

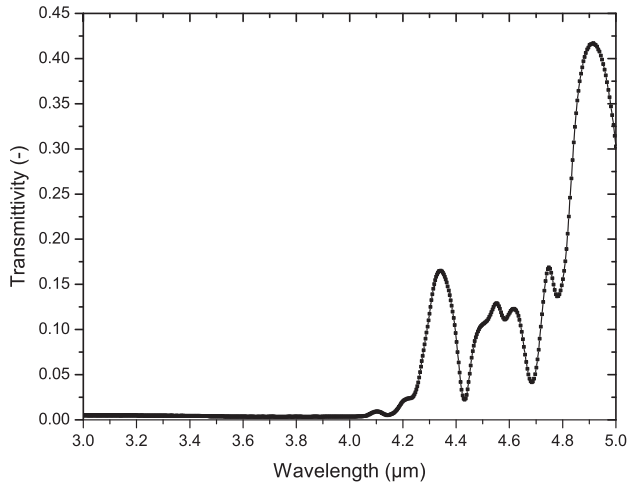


Fig. 3. Spectral transmittivity of ethanol as a function of the wavelength for an optical thickness of 1 mm ($T_{room} = 25\text{ °C}$).

$$\epsilon = 1 - e^{-k_{SW} \cdot x} \quad (10)$$

where x is the fluid thickness and ϵ is the global fluid emissivity. The constant ' k_{SW} ' for methanol is $3.02\text{ mm}^{-1} \pm 3.3\%$, for ethanol is $1.85\text{ mm}^{-1} \pm 2.1\%$ and for FC-72 is $0.783\text{ mm}^{-1} \pm 2.2\%$. To be able to make useful observations of liquids using an infrared camera, they need to be semi-transparent since:

- if the transmittivity is low (close to 0), it means the absorptivity is high (close to 1), so the fluid absorbs the heat flux by radiation and then the heat is transmitted to the next layer by re-emission. Through the whole liquid layer, little heat flux is transmitted directly to the camera and the global emissivity is high. However, a very low global signal is not useful to perform observations of the thermal motion of the fluid since only the drop interface is measured.
- if the transmittivity is high (close to 1), it means the absorptivity is low (close to 0), so the fluid does not absorb the heat flux by radiation and the heat flux density goes through the fluid without heating it. Through the whole liquid layer, the heat flux density is almost fully transmitted directly to the camera and the global emissivity is low. However, a very low signal from the liquid is not useful to perform observations of the thermal motion of the fluid since only the substrate temperature is measured.

3. Thermal motion and evaporation of drops

The complete evaporation process of semi-transparent sessile drops with the boundary condition on the temperature of the substrate is discussed in this section. This includes information from the observation of the drop shape from the side with the visible camera, from above with the infrared camera and from below thanks to the fluxmeter. Observations have been performed using ethanol, methanol and FC-72.

3.1. Mechanisms of drop evaporation

Initially the substrate is at a constant temperature. This is checked by the first image taken with the infrared camera. The heating block regulation system is on to avoid temperature decrease during the drop evaporation. Before the beginning of the experiment, the fluxmeter provides the natural convection heat flux on the heating substrate.

For all the fluids analyzed, we can observe that the process of evaporation is composed of three phases:

- Phase 1 – Warming up of the drop – The start of the experiment is defined as the initial contact of the drop on the substrate which is characterized by a sharp increase of the heat flux. The first seconds of the experiments are characterized by a transitional phenomenon. The drop, which was initially at room temperature, is placed on a warm surface and is first heated to reach almost the substrate temperature. The first step of the phenomenon is thus only driven by the heat capacity of the fluid.
- Phase 2 – Drop evaporation – The heat flux reaches a maximum value which corresponds to the beginning of our evaporation investigation. During this principal phase of evaporation, we can observe the appearance and the evolution of thermal-convective instabilities. The heat flux during over phase decrease continuously. Depending on the fluid, different kinds of these instabilities seem to be observed.
- Phase 3 – Film evaporation – A second phase of evaporation is characterized by the decrease of the heat flux when the convection cells have disappeared. The shape of the drop looks more like a layer than a drop. The evaporation rate is thus closer to film evaporation than drop evaporation.

The case an ethanol evaporating drop based on infrared visualization, the heat-flux and temperature measurements is presented. The results are summarized in Fig. 4 which shows the different phases of the evaporation of an ethanol drop on a substrate at a constant temperature of 48 °C . The three phases are separated thanks to the thermal flux signal. Assuming a substrate temperature at 50 °C and a room temperature at 25 °C ; without any drop on the substrate, the natural convection power transferred is 10 mW . With a 4 mm -diameter drop on the substrate, the remaining natural convection power transferred is 8 mW around the drop. Consequently, when the drop evaporate, this slight change in the natural convection heat flux cannot be observed in Fig. 4. Variations observed with Fig. 4 are mainly linked to the evaporation heat flux.

3.2. What can be observed depending on the fluid?

We present three experimental images of fluid dynamics for the three different liquids observed with one objective: to show the complexity of drop evaporation mechanisms. The three images have been extracted during all the phases of the drop evaporation (Figs. 5–7).

In the case of methanol (Fig. 5), numerous convection cells can be observed near the perimeter of the drop in a relative thin corona compared to the ethanol drop. At the center of the drop which is colder, the flow is much more unstable. The thermal flow motion inside the drop is fast compared to the other fluids. This point is very probably linked to the fluid viscosity which much smaller but need to be quantitatively checked. We can also observe that when the cold region is unstable and moves into the center, the convection cells rotate from the furthest point of the cold area to the closest point. The flow motion inside the drop stops when the drop reaches about 2 mm in diameter. Then the drop evaporate very slowly compared to the stages of the evaporation.

In the case of ethanol (Fig. 6), the same structure in cells is observed with a cold region located in the middle of the drop where the flow motion is more stable than in the methanol situation. Here also convection cells are observed near the drop perimeter but in a smaller quantity and in a wider corona. Then, during the evaporation, the flow motion changes very quickly and becomes large convection cells inside the drop. The total time of evaporation

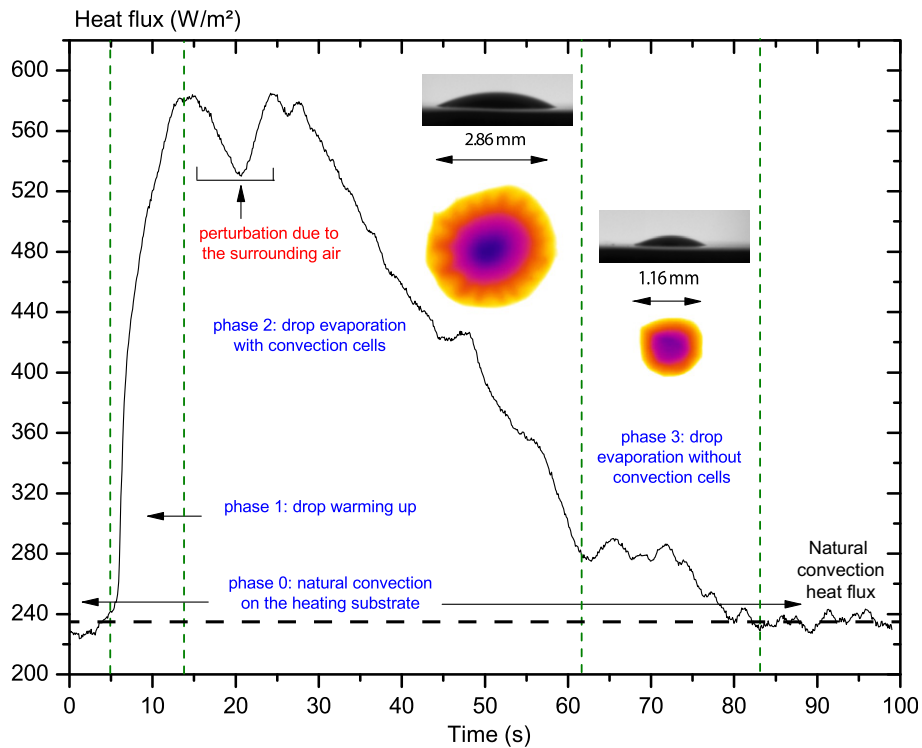


Fig. 4. Heat flux evolution during the evaporation of a ethanol sessile drop ($T_{room} = 28\text{ }^{\circ}\text{C}$, $T_{sub} = 48\text{ }^{\circ}\text{C}$, uncertainty on the heat flux is $\pm 10\text{ W/m}^2$).

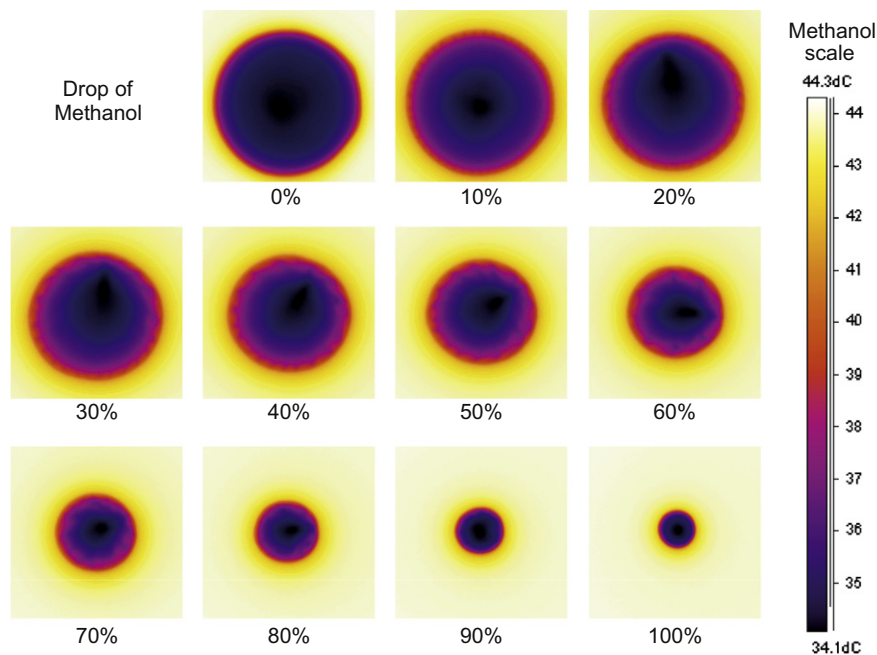


Fig. 5. Infrared sequence of methanol drops (% of total time of evaporation) ($T_{room} = 28 \pm 0.2\text{ }^{\circ}\text{C}$, $T_{sub} = 44 \pm 0.5\text{ }^{\circ}\text{C}$, drop diameter: 5.8 mm, uncertainty on the IR temperature scale is $\pm 0.5\text{ }^{\circ}\text{C}$).

is almost the same as that of methanol since the heat of vaporization is comparable.

In the case of FC-72 (Fig. 7), the latent heat of vaporization is about 10 times smaller than that of methanol and ethanol. Consequently, the drop evaporation time is short compared to the other two liquids. During the evaporation of FC-72, the stage of the evaporation evidence the same pattern than observed with ethanol and methanol then quickly the flow motion become different: we

discern multiple internal convective cells structures. This is completely different from the case of methanol and ethanol evaporation dynamics. This flow motion in the drop almost disappear after 60% of the drop evaporation time for a stable layer which evaporation by only conduction.

For fluids with even a comparable latent heat of vaporization, the thermal flow motion inside the drop can be very different since the fluid viscosity is the only important difference in the physical

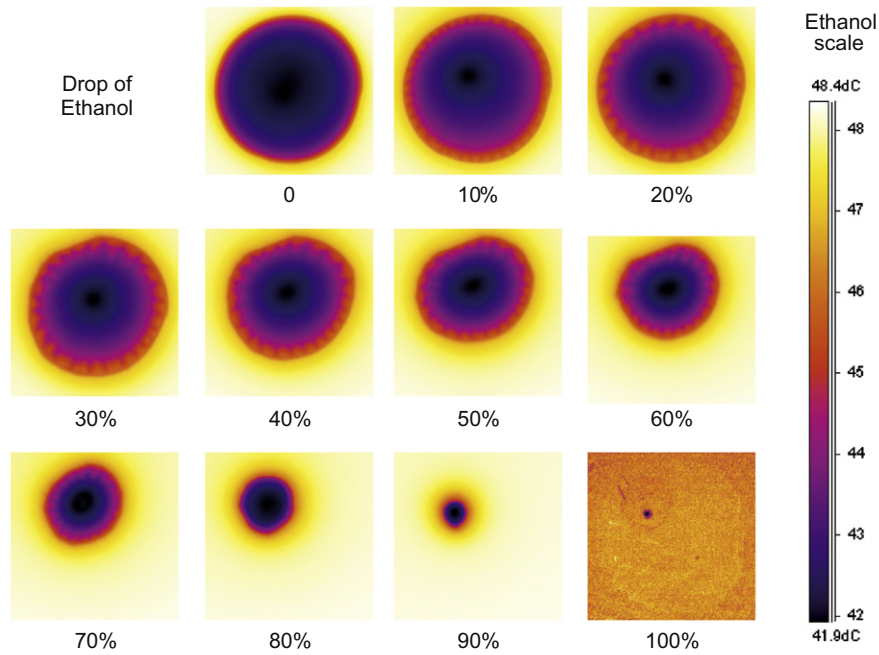


Fig. 6. Infrared sequence of ethanol drops (% of total time of evaporation) ($T_{room} = 28 \pm 0.2$ °C, $T_{sub} = 46 \pm 0.5$ °C, drop diameter: 4.3 mm, uncertainty on the IR temperature scale is ± 0.5 °C) (see movie online).

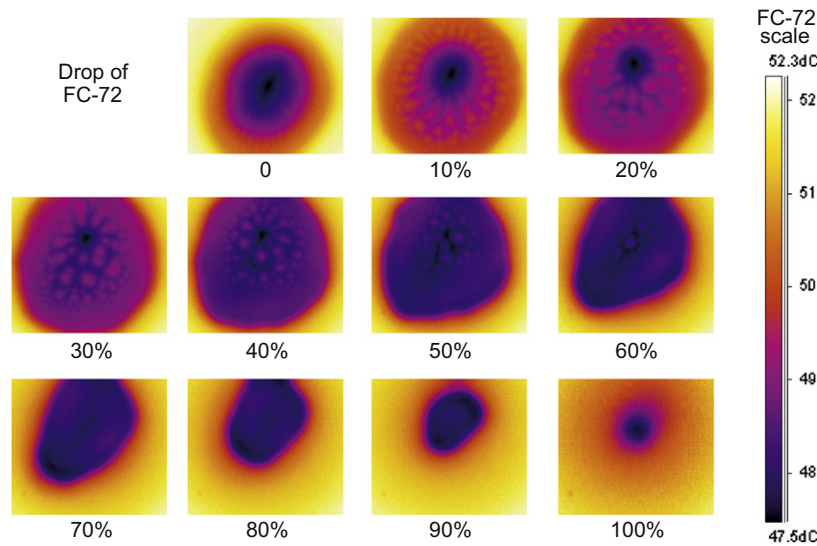


Fig. 7. Infrared sequence of FC-72 drops (% of total time of evaporation) ($T_{room} = 28 \pm 0.2$ °C, $T_{sub} = 51 \pm 0.5$ °C, drop diameter: 7.6 mm, uncertainty on the IR temperature scale is ± 0.5 °C).

properties of the fluid. With the knowledge of the temperature scale, it is possible to relate the temperature difference inside the drop (as much as 10 °C for methanol) to the quick flow motion; whereas for the ethanol drop, the maximum temperature difference is only 5 °C. For a fluid with a very low heat of vaporization (FC-72 for example), the dynamics of evaporation is completely different with almost no thermal patterns inside the drop during the main phase of evaporation. The evaporation of a drop of FC-72 is closer to that of a layer of FC-72, which is another area of research.

Different physical phenomena observed can be deduced wrongly from infrared camera observation without the knowledge of the infrared properties of the fluid. As we explained above, all

investigated fluids have a different “skin penetration depth” to infrared in the range of 3–5 μm . What may be attributed to different flow motions inside the drops could simply correspond to the observation of different information.

With Figs. 5 and 6, we can observe similar behaviours for ethanol and methanol since the two fluids have the same capillary lengths (1.71 mm for methanol and 1.69 mm for ethanol). In the case of the ethanol drop, the convection cells are wider compared to methanol and evolve slowly compared to the methanol situation. The methanol drop evidence a cold central area which is much more wider in the case of ethanol. Since both drops have the same dimensions and almost the same physical properties, the only difference is the Prandtl number which is 6.98 for methanol and 22.3 for ethanol.

The ratio of Prandtl number for these fluids is over 3, which indicate a better heat transfer by convection than conduction in the case of ethanol.

3.3. Non-dimensional analysis

Relevant dimensionless numbers are calculated to show the driving phenomenon. The Marangoni and the Rayleigh number are calculated based on equations below where ΔT is the temperature difference between the substrate and the room temperature; h and L are the vertical and radial dimensions of the drop; ρ , ν and κ are respectively the density, the kinematic viscosity and thermal diffusivity of the fluid, g is the gravitational constant, α is the coefficient of thermal expansion and the γ is the surface tension coefficient.

$$Ma = \frac{\gamma h^2 \Delta T}{\rho \nu \kappa L} \quad (11)$$

$$Ra = \frac{\alpha g h^4 \Delta T}{\nu \kappa L} \quad (12)$$

$$Bo = \frac{h^2 g \Delta \rho}{\sigma} \quad (13)$$

For a typical situation encountered in this manuscript which is an ethanol drop of 4 mm in diameter and 1 mm in height with a temperature difference of 25 °C; the Marangoni number is 1.41×10^4 , the Rayleigh number is 1.44×10^3 , the static Bond number is 0.366. For our situation, the capillary forces are dominating inside the drop and the Rayleigh and Marangoni numbers indicate the very probable existence of thermo-capillary instabilities.

3.4. Influence of the substrate temperature on the convection cells

In this section, we present results obtained by studying the influence of the substrate temperature on the number of convection cells for the case of ethanol. This can only be performed under certain conditions: the thickness of the fluid needs to be appropriate for the infrared visualization. For example, when working with ethanol, the height of the drop must not exceed 1 mm to allow the visualization of the cell through the whole thickness of the fluid.

The number of convection cells evolves during the drop evaporation: they appear a short time after the drop is placed and disappear when the drop becomes a layer. Fig. 8 shows the behaviour of

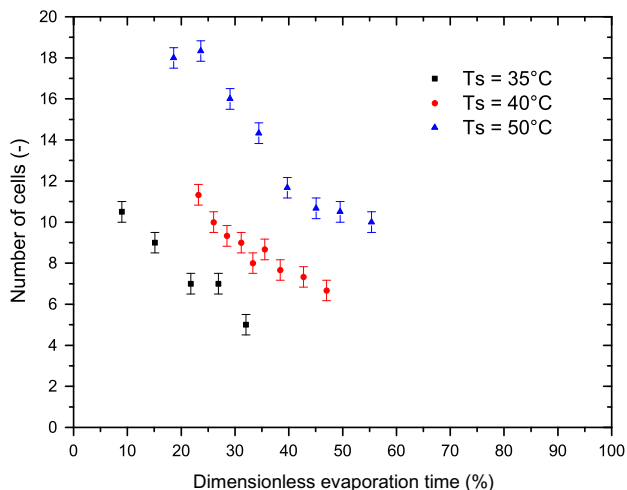


Fig. 8. Number of thermo-convective cell evolution for different substrate temperatures with ethanol drops ($T_{room} = 25$ °C).

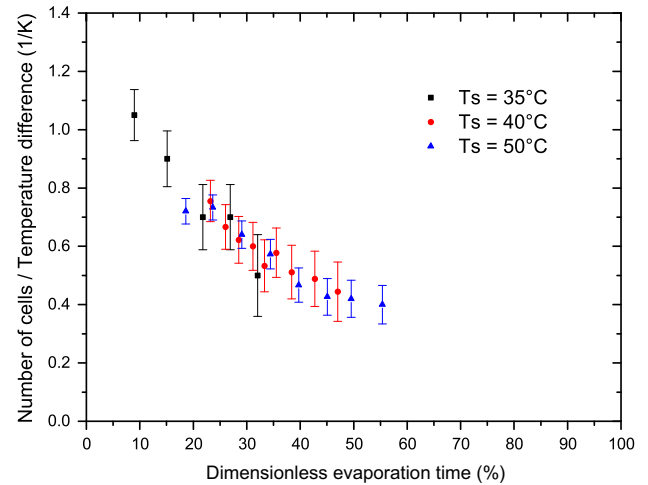


Fig. 9. Number of thermo-convective cell per temperature difference evolution for different substrate temperatures with ethanol drops ($T_{room} = 25$ °C).

the number of convection cells over time during the evaporation for three substrate temperatures: 35 °C, 40 °C and 50 °C. All experiments were performed on PTFE with a room temperature of 25 °C; also the initial size of the drop was the same with a diameter of 4 mm and a height of 1 mm. The number of convection cells increases with increasing surface temperature. Thereafter, we work with the temperature difference between the substrate and the room; three temperature differences were investigated: 10 °C, 15 °C and 25 °C. The decreasing behaviour of the number of cells is not linear for the three sets of data.

The number of convection cells should be related to the difference between the temperature of the substrate and the room temperature. In Fig. 9 we plot the number of convection cells divided by the temperature gradient as a function of the total time of evaporation in percentage. A good scaling for the three sets of data is obtained and evidence the non linear behaviour of the decrease in the number of convection cells during the evaporation. Concerning the time of appearance and disappearance of the convective cells, it is still not possible to relate these times to the evaporation process.

4. Conclusions

Analysis of sessile drop evaporation performed using an infrared camera evidences the existence of three steps during the evaporation process: first a warm-up phase, second evaporation with thermal-convective instabilities and finally evaporation without thermal patterns. The principal phase is characterized by the presence of 'convection cells'. For ethanol, we relate the decrease in convection cells during evaporation to the heat flux transferred to the drop which is measured by means of a heat fluxmeter. The link between the two factors needs to be investigated in more detail.

Furthermore, the behaviour of these convection cells has been related to the temperature difference between the heating substrate and the room temperature: a scaling law is obtained and evidence a power law variation. The paper also presents spectrophotometry measurements performed on ethanol, methanol and FC-72 in the range of 3–5 μm . This characterization is essential to perform quantitative measurement of the temperature variation along the interface. Further investigations need to be done to characterize these instabilities (threshold of appearance and disappearance, nature, ...). Also the coupling with the heat fluxmeter should

be studied carefully to check the link between the heat transfer to the drop and the mass flux of evaporation.

Acknowledgments

This research was supported by CNES (French National Space Agency) in the frame of a grant on “Sessile Drop Evaporation”.

Appendix A. Supplementary material

Supplementary data associated with this article can be found, in the online version, at [doi:10.1016/j.expthermflusci.2010.12.004](https://doi.org/10.1016/j.expthermflusci.2010.12.004).

References

- [1] V.A. Kuz, Evaporation of small drops, *J. Appl. Phys.* 10 (15) (1991) 7034–7036.
- [2] K.S. Birdi, D.T. Vu, A. Winter, A study of the evaporation rates of small water drops placed on a solid surface, *J. Phys. Chem.* 93 (9) (1989) 3702–3703.
- [3] K.S. Birdi, D. Vu, Wettability and the evaporation rates of fluids from solids surfaces, *J. Adhes. Sci. Technol.* 7 (6) (1993) 485–493.
- [4] F. Brochard, P.G. De Gennes, Spreading laws for liquid polymer droplets: interpretation of the foot, *J. Phys. Lett.* 45 (1984) 597–602.
- [5] H. Hu, R.G. Larson, Evaporation of a sessile droplet on a substrate evaporation of a sessile droplet on a substrate, *J. Phys. Chem. B* 6 (106) (2002) 1334–1344.
- [6] O.E. Ruiz, W.Z. Black, Evaporation of water droplets placed on a heated horizontal surface, *J. Heat Transfer* 124 (2002) 854–863.
- [7] R.D. Deegan, O. Bakajin, T.F. Dupont, G. Huber, S.R. Nagel, T.A. Witten, Contact line deposits in an evaporating drop, *Phys. Rev. E* 62 (1) (2000) 756–765.
- [8] A.P. Boyes, A.B. Ponter, Wettability of copper and polytetrafluoroethylene surfaces with water: the influence of environmental conditions, *Chem. Eng. Technol.* 45 (1973) 1250–1256.
- [9] R.G. Picknett, R. Bexon, The evaporation of sessile or pendant drops in still air, *J. Colloid Interface Sci.* 61 (2) (1977) 336–350.
- [10] C. Bourges-Monnier, M. Shanahan, Influence of evaporation on contact angle, *Langmuir* 11 (1995) 2820–2829.
- [11] J.J. Hegseth, N. Rashidnia, A. Chai, Natural convection in droplet evaporation, *Phys. Rev. E* 54 (2) (1996) 1640–1644.
- [12] S. Chandra, M. di Marzo, Y.M. Qiao, P. Tartarini, Effect of liquid–solid contact angle on droplet evaporation, *Fire Safety J.* 27 (1996) 141–158.
- [13] J.D. Bernardin, I. Mudawar, C.B. Walsh, E.I. Franses, Contact angle temperature dependence for water droplets on practical aluminum surfaces, *Int. J. Heat Mass Transfer* 40 (5) (1997) 1017–1033.
- [14] N. Zhang, D.F. Chao, A new laser shadowgraphy method for measurements of dynamic contact angle and simultaneous flow visualization in a sessile drop, *Opt. Laser Technol.* 34 (3) (2002) 243–248.
- [15] H.Y. Erbil, G. Mchale, M.I. Newton, Drop evaporation on solid surfaces: constant contact angle mode, *Langmuir* 18 (7) (2002) 2636–2641.
- [16] E.F. Crafton, W.Z. Black, Heat transfer and evaporation rates of small liquid droplets on heated horizontal surfaces, *Int. J. Heat Mass Transfer* 47 (2004) 1187–1200.
- [17] R. Savino, S. Fico, Transient Marangoni convection in hanging evaporating drops, *Phys. Fluids* 16 (10) (2004) 3738–3754.
- [18] L. Grandas, C. Reynard, R. Santini, L. Tadriss, Experimental study of the evaporation of a sessile drop on a heat wall. Wetting influence, *Int. J. Therm. Sci.* 44 (2005) 137–146.
- [19] C. Poulard, G. Guena, A.M. Cazabat, Diffusion-driven evaporation of sessile drops, *J. Phys. Condens. Matter* 17 (2005) 4213–4227.
- [20] J. Frassy, C. Lecot, C. Delattre, A. Soucemarianadin, Droplet evaporation on solid substrates of different wetting behaviour, *SHF Microfluidics 2006*, vol. 1, 2006, p. 12.
- [21] C. Sodtke, V.S. Ajaev, P. Stephan, Evaporation of thin liquid droplets on heated substrate, *Heat Mass Transfer* 43 (2007) 649–657.
- [22] L. Tarozzi, A. Muscio, P. Tartarini, Experimental tests of dropwise cooling in infrared-transparent media, *Exp. Therm. Fluid Sci.* 31 (2007) 857–865.
- [23] E. Widjaja, M.T. Harris, Numerical study of vapor phase–diffusion driven sessile drop evaporation, *Comput. Chem. Eng.* 32 (2008) 2169–2178.
- [24] K. Sefiane, J.R. Moffat, O.K. Matar, R.V. Craster, Self-excited hydrothermal waves in evaporating sessile drops, *Appl. Phys. Lett.* 93 (2008).
- [25] P. Tartarini, M.A. Corticelli, L. Tarozzi, Dropwise cooling: experimental tests by infrared thermography and numerical simulations, *Appl. Therm. Eng.* 29 (2009) 1391–1397.
- [26] L. Y Barash, T. P Bigioni, V.M. Vinokur, L. N Shchur, Evaporation and fluid dynamics of a sessile drop of capillary size, *Phys. Rev. E* 79 (2009) 046301.
- [27] D. Tam, V. Arnim, G.H. McKinley, A.E. Hosoi, Evaporation and fluid dynamics of a sessile drop of capillary size, *Phys. Rev. E* 79 (2009) 046301.
- [28] H.K. Dhavaleswarapu, C.P. Migliaccio, S.V. Garimella, J.Y. Murthy, Experimental investigation of evaporation from low-contact-angle sessile droplets, *Langmuir* 26 (2) (2009) 880–888.
- [29] V. Nikolayev, Dynamics of the triple contact line on a non-isothermal heater at partial wetting, *Phys. Fluids* 22 (2010) 082105.
- [30] N. Shahidzadeh-Bonn, S. Rafa, A. Azouni, D. Bonn, Evaporating droplets, *J. Fluid Mech.* 549 (2006) 07–313.
- [31] K.H. Kang, S.J. Lee, C.M. Lee, Visualization of flow inside a small evaporating droplet, in: 5th International Symposium on Particle Image Velocimetry, 2003.
- [32] R. Tuckermann, S. Bauerecker, H.K. Cammenga, IR-thermography of evaporating acoustically levitated drops, *Int. J. Thermophys.* 26 (2) (2005).
- [33] E. Wulsten, G. Lee, Surface temperature of acoustically levitated water microdroplets measured using infrared thermography, *Chem. Eng. Sci.* (2008). 1016/j.ces.2008.07.020.
- [34] X. Fang, B. Li, E. Petersen, Y. Ji, J.C. Sokolov, M.H. Rafailovich, Factors controlling the drop evaporation constant, *J. Phys. Chem. B* 109 (43) (2005) 20554–20557.